
Article:
You, Y, Zhang, L, Yang, M et al. (2022) Structured OMP for IRS-aided mmWave Channel Estimation by Exploiting Angular Spread. IEEE Transactions on Vehicular Technology, 71 (4). pp. 4444-4448. ISSN: 0018-9545

https://doi.org/10.1109/TVT.2022.3142285

Structured OMP for IRS-assisted mmWave Channel Estimation by Exploiting Angular Spread

You You, Li Zhang, *Senior Member, IEEE*, Minhua Yang, Yongming Huang, *Senior Member, IEEE*, Xiaohu You, *Fellow, IEEE*, and Chuan Zhang, *Senior Member, IEEE*

***Abstract*—An emerging technology namely the intelligent reflecting surface (IRS) can be deployed in millimeter wave (mmWave) communication to overcome the large propagation loss and huge power consumption issues. However, the large number of passive IRS elements without signal processing abilities induces high pilot overhead for channel estimation (CE). In this paper, the angular spread feature (or cluster feature) is exploited to formulate the CE problem as a structured sparse signal recovery problem. Then, a structured orthogonal matching pursuit (S-OMP) algorithm is proposed to efficiently solve the problem by utilizing the structure of the channel matrix in row and column without a priori knowledge of the angular spread. Simulation results demonstrate that S-OMP reduces about 40% to 50% pilot overhead at low signal-to-noise ratio (SNR) (SNR= 0 dB) while maintaining the same accuracy of CE compared with the existing methods.**

***Index Terms*—Intelligent reflecting surface (IRS), channel estimation, angular spread, orthogonal matching pursuit (OMP).**

I. Introduction

INTELLIGENT reflecting surface (IRS) system has attracted increasing attentions as a sustainable way for wireless connection [1]. Specifically, IRS is a kind of electromagnetic metasurfaces consisting of a large number of passive reflecting units. By adjusting the reflecting coefficients, signal propagation can be altered smartly to strengthen the desired signal efficiently without any radio frequency chains. IRS has been applied in various fields including mmWave communication [2]–[4]. But, channel estimation (CE) for IRS-assisted mmWave system is challenging due to the massive number of passive elements without signal processing capabilities.

The recently proposed IRS channel estimation approaches can be divided into separable cascaded channel estimation (two-stage channel estimation) [5] and direct cascaded channel estimation. In this paper, we focus on the direct channel estimation. The downlink cascaded CE problem is formulated to a sparse signal recovery problem in [4] and orthogonal matching pursuit (OMP) algorithm is employed to estimate the channel state information (CSI). A structural channel matrix induced by the shared scatterers is introduced and a double-structured orthogonal matching pursuit algorithm (DS-OMP) is proposed for the uplink CE in [6]. Although the sparsity and compressive sensing (CS) methods are utilized in both [4], [6], the pilot overhead is still high.

In addition to the sparse channel scattering, real-world channel measurements in mmWave communication have shown angular spread in terms of the root mean-squared (RMS) beam spread [7]. However, considering the high computational complexity caused by the high dimension of the cascaded channels, the existing mmWave CE methods ([8], [9]) utilizing the angular spread can not be applied in IRS-assisted systems.

In this paper, a structured orthogonal matching pursuit (S-OMP) algorithm is proposed for IRS-assisted mmWave CE by exploiting angular spread. The main novelties of this paper are summarized as follows:

1) By analyzing the impact of the angular spread on the cascaded channels, CE problem is formulated as a structured sparse signal recovery problem. To the best of our knowledge, this is the first attempt to exploit the angular spread feature in the IRS-assisted mmWave CE.
2) S-OMP is proposed to estimate the CSI without a prior information of the angular spread. Numerical simulations demonstrate that, without inducing more computational complexity, S-OMP can reduce about 40% to 50% pilot overhead while achieving the same accuracy of CE at low signal-to-noise ratio (SNR) (SNR=0 dB) compared with the existing methods.

II. System Model with Angular Spread

A. Channel Model

As shown in Fig. 1, we consider the scenario that the direct channel from user to base station (BS) is blocked by obstacles and IRS is employed to enable the connection. BS and IRS are equipped with N-antenna uniform linear array (ULA) and M-element uniform planer array (UPA), respectively, to serve a single user with single antenna. In Fig. 1, a, b and c, d represent the clusters with AoA angular spread at IRS and BS, respectively. $\mathbf{G} \in \mathbb{C}^{N\times M}$ and $\mathbf{h}_r \in \mathbb{C}^{M\times 1}$ are denoted as the IRS to BS channel and the user to IRS channel, respectively.

This work was supported in part by NSFC under Grants 62122020 and 61871115, in part by the Jiangsu Provincial NSF under Grant BK20211512, in part by the Nanjing Postdoctoral Recruitment Funds, and in part by the Fundamental Research Funds for the Central Universities. *(Corresponding author: Chuan Zhang.)*

Y. You, Y. Huang, X. You, and C. Zhang are with the LEADS of Southeast University, the National Mobile Communications Research Laboratory Southeast University, and Purple Mountain Laboratories, Nanjing 211189, China (email: chzhang@seu.edu.cn).

M. Yang is with the Purple Mountain Laboratories, Nanjing 211100, China.

L. Zhang is with the School of Electronic and Electrical Engineering, University of Leeds, Leeds LS2 9JT, U.K..

A narrowband geometric channel model [6] is adopted to characterize $\mathbf{G}$ as

$$\mathbf{G}=\sqrt{\frac{MN}{L_G}}\sum_{\ell_1=1}^{L_G}\sum_{i=1}^{I_{\ell_1}}\alpha_{\ell_1,i}\mathbf{a}_B\left(\theta^r_{\ell_1,i}\right)\mathbf{a}_I^T\left(\phi^t_{\ell_1},\rho^t_{\ell_1}\right), \tag{1}$$

where L_G is the number of clusters between the IRS and BS, I_{ℓ_1} represents the length (quantized angle) of the angular spread for the ℓ_1th cluster. $\alpha_{\ell_1,i}$, $\theta^r_{\ell_1,i}$ and $\phi^t_{\ell_1}/\rho^t_{\ell_1}$ denote the complex channel gain consisting of path loss, the spatial angle of the AoA with the i-th quantized angular point in the angular spread of the ℓ_1-th cluster at the BS and the spatial angle of the azimuth /elevation AoD of the ℓ_1-th cluster at the IRS, respectively. $\mathbf{a}_B$ and $\mathbf{a}_I$ are the normalized array steering vector for the BS and IRS, respectively. Specifically, $\mathbf{a}_B$ and $\mathbf{a}_I$ can be represented as

$$\begin{aligned}&\mathbf{a}_B(\theta)=\frac{1}{\sqrt{N}}[e^{j2\pi\theta\mathbf{n}}]^T \text{ with } \theta=\frac{d\cos\left(\theta_{physical}\right)}{\lambda}, \text{ and}\\ &\mathbf{a}_I(\phi,\rho)=\frac{1}{\sqrt{M}}[e^{j2\pi\rho\mathbf{m}_x}]^T\otimes[e^{j2\pi\phi\mathbf{m}_y}]^T \text{ with}\\ &\rho=\frac{d\cos\left(\rho_{physical}\right)}{\lambda},\phi=\frac{d\cos\left(\phi_{physical}\right)\sin\left(\rho_{physical}\right)}{\lambda},\end{aligned} \tag{2}$$

where λ is the wavelength, d is the antenna spacing, $\mathbf{n}=[0,1,\ldots,N-1]$, $\mathbf{m}_x=[0,1,\ldots,M_x-1]$, $\mathbf{m}_y=[0,1,\ldots,M_y-1]$. $\theta_{physical}$, $\phi_{physical}$ and $\rho_{physical}$ are the physical angle at the BS, the physical azimuth angle and the physical elevation angle at the IRS, respectively. θ, ϕ and ρ are the spatial angle of $\theta_{physical}$, $\phi_{physical}$ and $\rho_{physical}$, respectively. Similarly, $\mathbf{h}_r$ can be represented as

$$\mathbf{h}_r=\sqrt{\frac{M}{L_h}}\sum_{\ell_2=1}^{L_h}\sum_{j=1}^{J_{\ell_2}}\alpha_{\ell_2,j}\mathbf{a}_I(\phi^r_{\ell_2},\rho^r_{\ell_2}), \tag{3}$$

where L_h is the number of clusters between the UE and IRS, J_{ℓ_2} represents the length (quantized angle) of the angular spread for the ℓ_2-th cluster. $\alpha_{\ell_2,j}$, $\phi_{\ell_2,j}$ and $\rho_{\ell_2,j}$ denote the complex channel gain consisting of path loss, the spatial angle of the azimuth/elevation AoA with the j-th quantized angular point in the angular spread of the ℓ_2-th cluster at the IRS, respectively. For the same scatterer (cluster), the azimuth/elevation angular spread are considered the same.

The cascaded channel is defined as $\mathbf{H}\triangleq\mathbf{G}\mathtt{diag}(\mathbf{h}_r)$, where $\mathtt{diag}(\mathbf{h}_r)$ denotes the diagonal matrix with the vector $\mathbf{h}_r$ on its diagonal. Further, using the virtual channel representation [10], $\bar{\mathbf{H}}$ can be decomposed as

$$\mathbf{H}=\mathbf{D}_N\bar{\mathbf{H}}\mathbf{D}_M^T, \tag{4}$$

where $\mathbf{D}_N$ and $\mathbf{D}_M$ are $N\times N$ and $M\times M$ dictionary unitary matrices consisting of N steering vectors and M steering vectors of predetermined grids at the BS and IRS, respectively. We assume that all spatial angles are on the quantization grids. Then, $\bar{\mathbf{H}}$ is the sparse channel matrix in angular domain.

B. Problem Formulation

For the uplink CE, we assume that user sends pilot symbols $\mathbf{s}=[s_1,s_2,\ldots,s_P]$ successively to the BS via the IRS over P time slots as Fig. 1. In the p-th time slot, the IRS employs the reflecting coefficients denoted as $\boldsymbol{\psi}_p=[\psi_{p,1},\psi_{p,2},\ldots,\psi_{p,M}]$ and the received signal at the BS can be represented as

$$\begin{aligned}\mathbf{y}_p&=\mathbf{G}\mathtt{diag}(\boldsymbol{\psi}_p)\mathbf{h}_r s_p+\mathbf{n}_p=\mathbf{G}\mathtt{diag}(\mathbf{h}_r)\boldsymbol{\psi}_p s_p+\mathbf{n}_p\\&=\mathbf{H}\boldsymbol{\psi}_p s_p+\mathbf{n}_p,\end{aligned} \tag{5}$$

where $\mathbf{n}_p\sim\mathcal{CN}(0,\sigma_n^2)$ is the noise vector ($\mathcal{CN}(\mu,\sigma)$ denotes the probability density function of the circularly symmetric complex Gaussian distribution with mean μ and variance σ^2). Collecting $\mathbf{y}_p$ for all pilot symbols and assuming $s_p=1$, the received signal $\mathbf{Y}$ over P time slots can be formulated as

$$\mathbf{Y}=\mathbf{H}\boldsymbol{\Psi}+\mathbf{N}\overset{(a)}{=}\mathbf{D}_N\bar{\mathbf{H}}\mathbf{D}_M^H\boldsymbol{\Psi}+\mathbf{N}, \tag{6}$$

where $\boldsymbol{\Psi}=[\boldsymbol{\psi}_1,\ldots,\boldsymbol{\psi}_P]$, $\mathbf{N}=[\mathbf{n}_1,\ldots,\mathbf{n}_P]$ and the equality (a) is based on (4). In order to employ the CS algorithms [11], (6) can be rewritten as a CS problem as

$$\bar{\mathbf{Y}}=\bar{\boldsymbol{\Psi}}\bar{\mathbf{H}}_a+\bar{\mathbf{N}}, \tag{7}$$

where $\bar{\mathbf{H}}_a\triangleq\bar{\mathbf{H}}^H$, $\bar{\mathbf{Y}}\triangleq(\mathbf{D}_N^H\mathbf{Y})^H$ and $\bar{\boldsymbol{\Psi}}\triangleq(\mathbf{D}_M^H\boldsymbol{\Psi})^H$. Based on (7), compressive sensing algorithms such as OMP can be employed for CE [6].

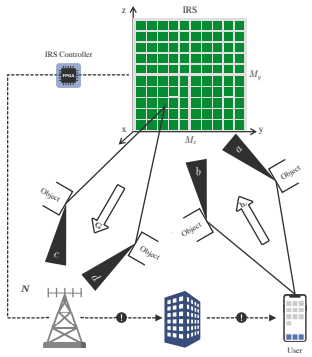

Fig. 1. System model.

III. Proposed Structured Algorithm for Channel Estimation

A. Derivation of the Structured Channel Matrix

We derive the formula of the cascaded channel, starting with the following lemma. Let $\circ$ note the 'Hadamard product' as $\mathbf{c}\circ\mathbf{d}=[c_1d_1,c_2d_2,\ldots,c_Nd_N]$, where $\mathbf{c}=[c_1,c_2,\ldots,c_N]$, $\mathbf{d}=[d_1,d_2,\ldots,d_N]$. Lemma 1 can be proved as following.

lemma 1: $\mathbf{a}_I(\theta_1,\beta_1)\circ\mathbf{a}_I(\theta_2,\beta_2)=\frac{1}{\sqrt{M}}\mathbf{a}_I(\theta_1+\theta_2,\beta_1+\beta_2)$,

Proof:

$$\begin{aligned}&\mathbf{a}_I(\theta_1,\beta_1)\circ\mathbf{a}_I(\theta_2,\beta_2)\\&=\frac{1}{\sqrt{M}}[e^{j2\pi\theta_1\mathbf{m}_x}]^T\otimes[e^{j2\pi\beta_1\mathbf{m}_y}]^T\circ\frac{1}{\sqrt{M}}[e^{j2\pi\theta_2\mathbf{m}_x}]^T\otimes[e^{j2\pi\beta_2\mathbf{m}_y}]^T\\&=\frac{1}{M}[e^{j2\pi\theta_1 m_{x,1}},e^{j2\pi\theta_1 m_{x,2}},\ldots,e^{j2\pi\theta_1 m_{x,M_x}}]^T\otimes[e^{j2\pi\beta_1\mathbf{m}_y}]^T\\&\quad\circ[e^{j2\pi\theta_2 m_{x,1}},e^{j2\pi\theta_2 m_{x,2}},\ldots,e^{j2\pi\theta_2 m_{x,M_x}}]^T\otimes[e^{j2\pi\beta_2\mathbf{m}_y}]^T\\&=\frac{1}{M}[e^{j2\pi\theta_1 m_{x,1}}e^{j2\pi\beta_1\mathbf{m}_y},\ldots,e^{j2\pi\theta_1 m_{x,M_x}}e^{j2\pi\beta_1\mathbf{m}_y}]^T\\&\quad\circ[e^{j2\pi\theta_2 m_{x,1}}e^{j2\pi\beta_2\mathbf{m}_y},\ldots,e^{j2\pi\theta_2 m_{x,M_x}}e^{j2\pi\beta_2\mathbf{m}_y}]^T\\&=\frac{1}{M}[e^{j2\pi(\theta_1+\theta_2)m_{x,1}}e^{j2\pi(\beta_1+\beta_2)\mathbf{m}_y},\ldots,\\&\quad e^{j2\pi(\theta_1+\theta_2)m_{x,M_x}}e^{j2\pi(\beta_1+\beta_2)\mathbf{m}_y}]^T\\&=\frac{1}{M}[e^{j2\pi(\theta_1+\theta_2)\mathbf{m}_x}]^T\otimes[e^{j2\pi(\beta_1+\beta_2)\mathbf{m}_y}]^T\\&=\frac{1}{\sqrt{M}}\mathbf{a}_I(\theta_1+\theta_2,\beta_1+\beta_2),\end{aligned} \tag{8}$$

where $\mathbf{a} \otimes \mathbf{b}$ denotes the Kronecker product of $\mathbf{a}$ and $\mathbf{b}$. Based on (1), (3) and lemma 1, the cascaded channel $\mathbf{H} = \mathbf{G}\mathtt{diag}(\mathbf{h_r})$ can be derived as

$$\begin{aligned}
\mathbf{H} &= \sqrt{\frac{MN}{L_G}} \sum_{\ell_1=1}^{L_G} \sum_{i=1}^{I_{\ell_1}} \alpha_{\ell_1,i} \mathbf{a}_B(\theta^r_{\ell_1,i}) \mathbf{a}_I^T(\phi^t_{\ell_1}, \rho^t_{\ell_1}) \\
&\quad \mathtt{diag}\left(\sqrt{\frac{M}{L_h}} \sum_{\ell_2=1}^{L_h} \sum_{j=1}^{J_{\ell_2}} \alpha_{\ell_2,j} \mathbf{a}_I(\phi^r_{\ell_2,j}, \rho^r_{\ell_2,j}) \right) \\
&\overset{(a)}{=} \sqrt{\frac{MN}{L_G}} \sum_{\ell_1=1}^{L_G} \sum_{i=1}^{I_{\ell_1}} \alpha_{\ell_1,i} \mathbf{a}_B(\theta^r_{\ell_1,i}) \mathbf{a}_I^T(\phi^t_{\ell_1}, \rho^t_{\ell_1}) \\
&\quad \circ \sqrt{\frac{M}{L_h}} \sum_{\ell_2=1}^{L_h} \sum_{j=1}^{J_{\ell_2}} \alpha_{\ell_2,j} \mathbf{a}_I^T(\phi^r_{\ell_2,j}, \rho^r_{\ell_2,j}) \\
&\overset{(b)}{=} \sqrt{\frac{MN}{L_G}} \sum_{\ell_1=1}^{L_G} \sum_{i=1}^{I_{\ell_1}} \alpha_{\ell_1,i} \mathbf{a}_B(\theta^r_{\ell_1,i}) \\
&\quad \sqrt{\frac{M}{L_h}} \sum_{\ell_2=1}^{L_h} \sum_{j=1}^{J_{\ell_2}} \alpha_{\ell_2,j} \mathbf{a}_I^T(\phi^t_{\ell_1}, \rho^t_{\ell_1}) \circ \mathbf{a}_I^T(\phi^r_{\ell_2,j}, \rho^r_{\ell_2,j}) \\
&\overset{(c)}{=} \sqrt{\frac{MN}{L_G L_h}} \sum_{\ell_1=1}^{L_G} \sum_{i=1}^{I_{\ell_1}} \sum_{\ell_2=1}^{L_h} \sum_{j=1}^{J_{\ell_2}} \alpha_{\ell_1,i} \alpha_{\ell_2,j} \mathbf{a}_B(\theta^r_{\ell_1,i}) \\
&\quad \mathbf{a}_I^T(\phi^t_{\ell_1} + \phi^r_{\ell_2,j}, \rho^t_{\ell_1} + \rho^r_{\ell_2,j}),
\end{aligned} \tag{9}$$

where the diagonalization is expressed by Hadamard product in equality (a), the equality (b) comes from the identity $A \circ (B + C) = A \circ B + A \circ C$, and the equality (c) is based on the lemma 1. Further, according to (4), $\bar{\mathbf{H}}$ can be presented as

$$\begin{aligned}
\bar{\mathbf{H}} &= \mathbf{D}_N^H \mathbf{H} \mathbf{D}_M^* \\
&= \sqrt{\frac{MN}{L_G L_h}} \sum_{\ell_1=1}^{L_G} \sum_{i=1}^{I_{\ell_1}} \sum_{\ell_2=1}^{L_h} \sum_{j=1}^{J_{\ell_2}} \alpha_{\ell_1,i} \alpha_{\ell_2,j} \widetilde{\mathbf{a}}_B(\theta^r_{\ell_1,i}) \\
&\quad \widetilde{\mathbf{a}}_I^T(\phi^t_{\ell_1} + \phi^r_{\ell_2,j}, \rho^t_{\ell_1} + \rho^r_{\ell_2,j}).
\end{aligned} \tag{10}$$

where $\widetilde{\mathbf{a}}_B(\theta^r_{\ell_1,i}) = \mathbf{D}_N^H \mathbf{a}_B(\theta^r_{\ell_1,i})$ and $\widetilde{\mathbf{a}}_I(\phi^t_{\ell_1} + \phi^r_{\ell_2,j}, \rho^t_{\ell_1} + \rho^r_{\ell_2,j}) = \mathbf{D}_M^H \mathbf{a}_I(\phi^t_{\ell_1} + \phi^r_{\ell_2,j}, \rho^t_{\ell_1} + \rho^r_{\ell_2,j})$.

B. Analysis of the Structural Channel Model

According to (10), it can be found that both $\widetilde{\mathbf{a}}_B(\theta^r_{\ell_1,i})$ and $\widetilde{\mathbf{a}}_I(\phi^t_{\ell_1} + \phi^r_{\ell_2,j}, \rho^t_{\ell_1} + \rho^r_{\ell_2,j})$ have only one non-zero element, which lies on the position of array steering vector at the direction $(\theta^r_{\ell_1,i})$ and direction $(\phi^t_{\ell_1} + \phi^r_{\ell_2,j}, \rho^t_{\ell_1} + \rho^r_{\ell_2,j})$. As a result, with limited scatterers (L_G, L_h) and angular spread, $\bar{\mathbf{H}}$ has common row-sparsity and column-sparsity. It is worth noting that, considering the size of the surface roughness and the small wavelength of mmWave, the diffusion scattering effect is more obvious and results in non-negligible angular spread (or clustering) feature compared with microwave communications. However, the scattering effect is based on the material properties, type of environment and physical parameters. Thus, a prior information of the angular spread (i.e. the quantized angular spread length I_{ℓ_1}, J_{ℓ_2}) is hard to be acquired.

More importantly, according to (2), it can be found that the adjacent physical angle $\theta_{physical} \in [0, \pi]$ results in adjacent spatial angle $\theta \in [-d/\lambda, d/\lambda]$ due to the monotonicity of the cosine function. As a result, the physical angular spread results in spatial angular spread (the adjacent physical angles result in adjacent spatial angles).

According to (10) and the spatial angular spread feature, the non-zero rows are divided into L_G blocks and each block has I_{ℓ_1} non-zero rows. Similarly, for each direction $(\phi^t_{\ell_1}, \rho^t_{\ell_1})$, the spatial angular spread of direction $(\phi^r_{\ell_2,j}, \rho^r_{\ell_2,j})$ results in L_h groups of non-zero columns and each group has J_{ℓ_2} non-zero columns. Note that, in each group, the non-zero columns are not adjacent and the spatial angular spread of direction $(\phi^r_{\ell_2,j}, \rho^r_{\ell_2,j})$ results in a column spacing of M_y+1 between the non-zero columns due to the Kronecker product calculation.

In the following, an example is used to illustrate the block-sparse structure of $\bar{\mathbf{H}}$ more clearly. First, we take the angular spread into account and generate channel $\mathbf{G}$ and channel $\mathbf{h}_r$ based on (1) and (3), respectively. Parameters of the channels are listed in Table. I. Then we calculate $\bar{\mathbf{H}}$ as $\mathbf{D}_N^H \mathbf{G} \mathtt{diag}(\mathbf{h}_r) \mathbf{D}_M^*$ and show the structure obtained from computer simulation in Fig. 2 where each entry of $\bar{\mathbf{H}}$ is represented as a square and the right figure is the the enlarged block 1. Fig. 2 proves the derivation and analysis of (10).

TABLE I
CHANNEL PARAMETERS OF THE EXAMPLE.

Channel parameters	Values
$(M, N), (M_x, M_y)$	$(256, 32), (16, 16)$
$(L_G, L_h), (I_1, I_2, I_3), (J_1, J_2)$	$(3, 2), (4, 4, 2), (3, 4)$

* L_G and L_h are the number of clusters in $\mathbf{G}$ and $\mathbf{h}_r$. (I_1, I_2, I_3) and (J_1, J_2) are the quantization length of the angular spread of each cluster at the BS and IRS, respectively.

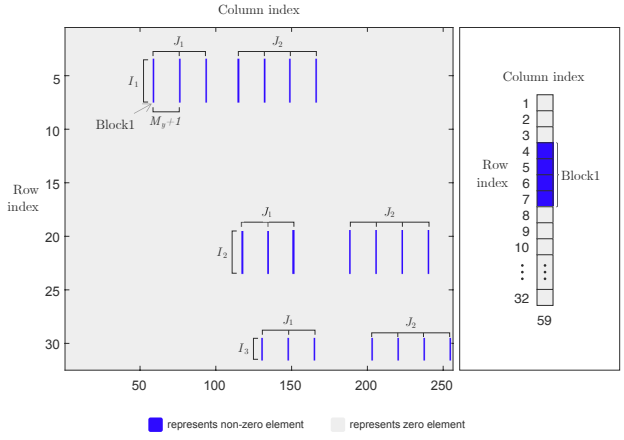

Fig. 2. Structure of $\bar{\mathbf{H}}$.

C. Proposed S-OMP Algorithm

In this subsection, we propose S-OMP algorithm to reduce the pilot overhead by utilizing the unique structure of $\bar{\mathbf{H}}$. Specifically, S-OMP requires measurement matrix $\bar{\mathbf{Y}}$, sensing matrix $\bar{\mathbf{\Psi}}$ and total number of the non-zero elements K. Output is the $\bar{\mathbf{H}}_a$ (note that $\bar{\mathbf{H}}_a = \bar{\mathbf{H}}^H$). Step 1 is for initialization.

Algorithm 1 S-OMP for IRS-aided mmWave CE

Input: $\bar{\mathbf{Y}}$, $\bar{\mathbf{\Psi}}$, K.
Output: $\bar{\mathbf{H}}_a$.
1: Initialization: $\Omega = \varnothing$, $\mathbf{r} = \bar{\mathbf{Y}}$, $\bar{\mathbf{H}}_a = \mathbf{0}$,$[:, M] = \text{size}(\bar{\mathbf{\Psi}})$, $[:, N] = \text{size}(\bar{\mathbf{Y}})$
2: **for** $l = 1 : K$ **do**
3: $\quad \mathbf{t} = |\bar{\mathbf{\Psi}}^H \mathbf{r}|$, $l_1 = l$
4: $\quad$ **while** $l_1 > 1$ **do**
5: $\quad\quad \mathbf{t}(\mathbf{L}(1, l_1 - 1), \mathbf{L}(2, l_1 - 1)) = \max(\mathbf{t})$
6: $\quad\quad l_1 = l_1 - 1$
7: $\quad$ **end while**
8: $\quad \bar{\mathbf{t}} = \text{couple}(\mathbf{t})$, $\bar{\mathbf{t}}_v = \text{vect}(\bar{\mathbf{t}})$, $l_2 = l$
9: $\quad$ **while** $l_2 > 1$ **do**
10: $\quad\quad \bar{\mathbf{t}}(\mathbf{L}(1, l_2 - 1), \mathbf{L}(2, l_2 - 1)) = 0$
11: $\quad\quad l_2 = l_2 - 1$
12: $\quad$ **end while**
13: $\quad n^* = \underset{i=1,\ldots,MN}{\arg\max}\ \bar{\mathbf{t}}_v(i)$
14: $\quad \Omega = \Omega \cup n^*$
15: $\quad \mathbf{C} = \text{ceil}(\Omega / M)$, $\mathbf{R} = \Omega - M(C - 1)$
16: $\quad \mathbf{L} = [\mathbf{R}; \mathbf{C}]$
17: $\quad \bar{\mathbf{C}} = \text{unique}(\mathbf{C})$
18: $\quad$ **for** $j = 1 : \max(\text{size}(\bar{\mathbf{C}}))$ **do**
19: $\quad\quad i = \text{find}(\mathbf{C} == \bar{\mathbf{C}}(j))$
20: $\quad\quad \bar{\mathbf{\Psi}}_s = \bar{\mathbf{\Psi}}(:, \mathbf{R}(i))$
21: $\quad\quad \bar{\mathbf{H}}_a(\mathbf{R}(i), \bar{\mathbf{C}}(j)) = \bar{\mathbf{\Psi}}_s^{\dagger} \bar{\mathbf{Y}}(:, \bar{\mathbf{C}}(j))$
22: $\quad$ **end for**
23: $\quad \mathbf{r} = \mathbf{r} - \bar{\mathbf{\Psi}} \bar{\mathbf{H}}_a$
24: **end for**

TABLE II
CUSTOM FUNCTIONS IN ALGORITHM. 1.

Functions	Definition
(a,b)=size($\mathbf{A}$)	a (b) are the row (column) dimension of $\mathbf{A}$.
$\bar{\mathbf{a}}$=couple($\mathbf{a}$)	$\bar{\mathbf{a}}$ is the modified coherence of $\mathbf{a}$ as defined in (11).
$\mathbf{a}$=vect($\mathbf{A}$)	$\mathbf{a}$ is the vectorized vector (in column) of matrix $\mathbf{A}$.
a=ceil(A)	a is the nearest integer greater than or equal to A.
$\mathbf{a}$=unique($\mathbf{A}$)	$\mathbf{a}$ has the same data as $\mathbf{A}$, but with no repetitions.
$\mathbf{a}$=find($\mathbf{A}$)	$\mathbf{a}$ contains the indices of nonzero elements in $\mathbf{A}$.

After initialization, S-OMP has K iterations. We first introduce the algorithm step by step for the first iteration.

- In step 3, the initial coherence $\mathbf{t}$ is calculated as $\mathbf{t} = |\bar{\mathbf{\Psi}}^H \mathbf{r}|$, where $\mathbf{t}(i, j) = t_{i,j}$ is the initial coherence of the (i, j)-th element. This step is the same as OMP.
- In step 8, the initial coherence $\mathbf{t}$ is further improved to a modified coherence $\bar{\mathbf{t}}$ by the coupling function as $\bar{\mathbf{t}} = \text{couple}(\mathbf{t})$. According to the structure of $\bar{\mathbf{H}}_a$, the coupling function couple$(\cdot)$ is defined as (11).

$$\begin{aligned} \bar{\mathbf{t}}(i, j) &= \text{couple}\big(\mathbf{t}(i, j)\big) \\ &= \mathbf{t}(i, j) + \beta_1 \mathbf{t}(i, j+1) + \beta_2 \mathbf{t}(i, j-1) \\ &= +\beta_3 \mathbf{t}(i + M_y + 1, j) + \beta_4 \mathbf{t}(i - M_y - 1, j), \end{aligned} \tag{11}$$

- In step 13-14, the index of element with the largest modified coherence in $\bar{\mathbf{t}}_v$ is added in set Ω.
- In step 15-16, the row index $\mathbf{R}$ and the column index $\mathbf{C}$ corresponding to the chosen support with the largest modified coherence can be obtained based on the index n^* in Ω. $\mathbf{L}$ is defined as a two-row matrix to store the row and column indices of the selected supports in each iteration.
- In step 17-22, the least square method is applied to estimate the channel gains. Because the coherences in the same column are calculated by the same row of $\bar{\mathbf{\Psi}}^H$, the channel gains of the selected support in the same column can be estimated together.
- In step 23, the contributions of the chosen column vectors to $\mathbf{r}$ are subtracted to update the residual.

For the l-th ($l > 1$) iteration, step 4-7 and step 9-12 need to be added.

- In step 4-7, because the impact of the previously estimated supports on the coherence is removed by step 23, the initial coherence of these supports are all zeros in the current iteration. To utilize the structure information by the coupling function, the coherence of these supports is set to $\max(\mathbf{t})$.
- In step 9-12, after calculating the modified coherence in step 8, the modified coherence of the previous selected supports need to be set as zeros again to guarantee that the previous selected supports will not be re-chosen.

By applying S-OMP, $\bar{\mathbf{H}}_a$ can be estimated according to (7). Then $\bar{\mathbf{H}}$ can be recovered as $\bar{\mathbf{H}} = \bar{\mathbf{H}}_a^H$.

D. Computational Complexity Analysis

The comparison of the computational complexity is listed in Table III. It is straightforward to find that the complexity of OMP algorithm solving (7) is $\mathcal{O}(KPMN)$ [11]. Compared with OMP, S-OMP has some additional operations including Step 8, Steps 4-7 and Steps 9-12 inducing $\mathcal{O}(4KMN)$, $\mathcal{O}(K + K^2)$ and $\mathcal{O}(K + K^2)$ computational complexity, respectively. In the IRS-assisted mmWave system, the computational complexity of S-OMP can be approximated as $\mathcal{O}(KPMN)$ when $MN \gg P > K$. The Row-OMP [12] estimates the common row index firstly and estimates the column index with L_h iterations. As a result, the computational complexity of Row-OMP is $\mathcal{O}(PN) + \mathcal{O}(L_h PMN)$ and can be approximated as $\mathcal{O}(L_h PMN)$.

TABLE III
COMPARISON OF THE COMPUTATIONAL COMPLEXITY.

Algorithms	Computational complexity
OMP	$\mathcal{O}(KPMN)$
S-OMP	$\mathcal{O}(KPMN) + \mathcal{O}(4KMN) + \mathcal{O}(2K + 2K^2) \approx \mathcal{O}(KPMN)$
Row-OMP	$\mathcal{O}(PN) + \mathcal{O}(L_h PMN) \approx \mathcal{O}(L_h PMN)$

* In the IRS-aided mmWave system, we have $MN \gg P > K = L_G L_h > L_h$.

IV. SIMULATION RESULTS

In this section, computer simulations are presented to evaluate performance of the proposed CE method. All the simulations are averaged over 500 channel realizations with 60 GHz carrier frequency. Each element of RIS reflecting

TABLE IV
SYSTEM PARAMETERS IN THE SIMULATIONS.

Parameters	Values
$(M,N),(M_x,M_y),(L_G,L_h)$	$(256,32),(16,16),(3,2)$
(d_{IB},d_{UI})	(10 m, 100 m)
$(\lvert\alpha_{l_1}\rvert,\lvert\alpha_{l_2}\rvert)$	$(10^{-3}d_{IB}^{-2.2},10^{-3}d_{UI}^{-2.8})$
Size of angular spread	$[5^\circ,20^\circ]$

* $d_{IB}=10$m and $d_{UI}=100$m represent the distance from the IRS to BS and the distance from the user to IRS, respectively.

matrix $\mathbf{\Psi}$ is selected from $\{-\frac{1}{\sqrt{N}},\frac{1}{\sqrt{N}}\}$ as in [6]. Other system parameters are listed in Table IV.

We compare the proposed S-OMP based CE method with OMP scheme [4], Row-OMP scheme [12] and Oracle OMP scheme, where the Oracle OMP scheme is assumed to have the perfect support knowledge of the channel matrix and provide the best achievable performance as the benchmark.

Fig. 3 shows the normalized mean square error (NMSE) versus pilots overhead P at 0 dB SNR, where the NMSE is defined as $10\log_{10}\left(\mathrm{E}(\|\mathbf{H}-\mathbf{H}^{\text{estimate}}\|_F^2/\|\mathbf{H}\|_F^2)\right)$. As shown, in order to achieve the same NMSE performance such as -14 dB, the proposed S-OMP requires only about 95 pilots which is nearly 50% less than OMP required (190 pilots) and nearly 40% less than Row-OMP required (160 pilots). Fig. 3 proves that the proposed S-OMP can significantly reduce pilot overhead for CE and approaches the benchmark that is achieved by oracle OMP at high pilot overhead.

Fig. 4 depicts the NMSE performance against the SNR from 0 dB to 20 dB, where 64 pilots are used. It is obvious that the NMSE performance of the proposed S-OMP approaches to that of the Oracle OMP and has evidently improved performance compared with the OMP and Row-OMP at low SNR (SNR <13 dB). The improvement is more significant at lower SNRs because the coupling support estimation in the S-OMP effectively mitigates the impact of the large noises. However, when the SNR is high (SNR >13 dB), these algorithms show very close performance. Considering that the SNR is variable and usually unknown in the practical communication systems, it is recommanded to apply S-OMP to achieve superior performance at low SNR and very similar performance to other existing methods at high SNR. In summary, S-OMP can achieve desirable CE accuracy with significantly reduced pilot overhead and without additional computational complexity.

V. CONCLUSION

In this paper, we proposed the S-OMP based CE method for the IRS-assisted mmWave system by utilizing the angular spread feature. Specifically, we formulated the CE problem as a structured sparse signal recovery problem and analyzed the structure of channel. Then, S-OMP was proposed to effectively solve the problem without additional computational complexity and a prior knowledge of angular spread. Simulation results show that our proposed method requires significantly fewer pilot overheads to achieve the same CE accuracy compared with other existing methods. In the future work, off-grid errors and multi-user multi-antenna system will be taken into account.

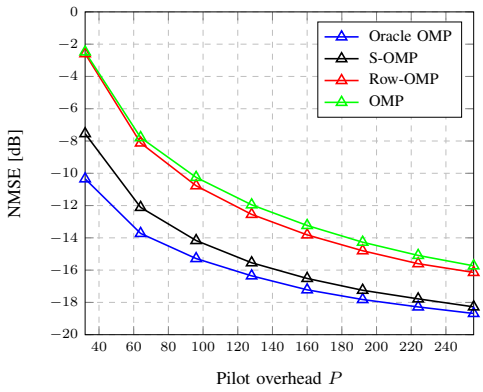

Fig. 3. NMSE performances v.s. pilot overhead P.

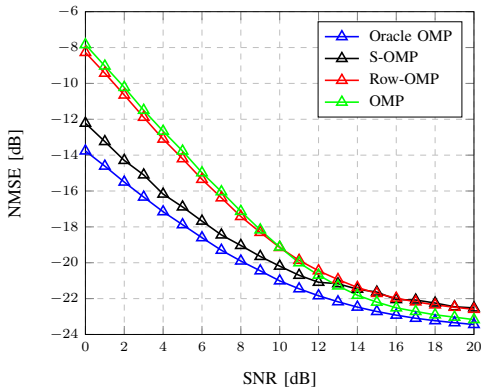

Fig. 4. NMSE performance v.s. SNR [dB].

REFERENCES

[1] Q. Wu and R. Zhang, "Towards smart and reconfigurable environment: Intelligent reflecting surface aided wireless network," *IEEE Commun. Mag.*, vol. 58, no. 1, pp. 106–112, Nov. 2019.

[2] C. Huang *et al.*, "Multi-hop RIS-empowered terahertz communications: A DRL-based hybrid beamforming design," *IEEE J. Sel. Areas Commun.*, vol. 39, no. 6, pp. 1663–1677, Jun. 2021.

[3] D. Zhang *et al.*, "Mobile user trajectory tracking for irs enabled wireless networks," *IEEE Trans. Veh. Technol.*, vol. 70, no. 8, pp. 8331–8336, Aug. 2021.

[4] P. Wang, J. Fang, H. Duan, and H. Li, "Compressed channel estimation for intelligent reflecting surface-assisted millimeter wave systems," *IEEE Signal Process. Lett.*, vol. 27, pp. 905–909, May 2020.

[5] L. Wei *et al.*, "Channel estimation for RIS-empowered multi-user MISO wireless communications," *IEEE Trans. Commun.*, Jun. 2021.

[6] X. Wei, D. Shen, and L. Dai, "Channel estimation for RIS assisted wireless communicationsPart II: An improved solution based on double-structured sparsity," *IEEE Commun. Lett.*, vol. 25, no. 5, pp. 1403–1407, Jan. 2021.

[7] T. S. Rappaport *et al.*, "Millimeter wave mobile communications for 5G cellular: It will work!" *IEEE Access*, vol. 1, pp. 335–349, May 2013.

[8] P. Wang *et al.*, "Sparse channel estimation in millimeter wave communications: Exploiting joint AoD-AoA angular spread," in *Proc. IEEE Int. Conf. Commun. (ICC)*, Paris, France, May 2017, pp. 1–6.

[9] X. Li, J. Fang, H. Li, and P. Wang, "Millimeter wave channel estimation via exploiting joint sparse and low-rank structures," *IEEE Trans. Wireless Commun.*, vol. 17, no. 2, pp. 1123–1133, Nov. 2017.

[10] A. M. Sayeed, "Deconstructing multiantenna fading channels," *IEEE Trans. Signal Process.*, vol. 50, no. 10, pp. 2563–2579, Nov. 2002.

[11] J. A. Tropp and A. C. Gilbert, "Signal recovery from random measurements via orthogonal matching pursuit," *IEEE Trans. Inf. Theory*, vol. 53, no. 12, pp. 4655–4666, Mar. 2007.

[12] J. Chen *et al.*, "Channel estimation for reconfigurable intelligent surface aided multi-user mimo systems," *arXiv preprint arXiv:1912.03619*, Dec. 2019.